THE ASTROPHYSICAL JOURNAL, 461:265–281, 1996 April 10

MASTER EQUATION STUDIES OF COLLISIONAL EXCITATION AND DISSOCIATION OF H_2 MOLECULES BY H ATOMS

P. G. MARTIN
Canadian Institute for Theoretical Astrophysics, University of Toronto, Toronto, ON M5S 3H8, Canada; pgmartin@cita.utoronto.ca
D. H. SCHWARZ
Institute of Astronomy, The Observatories, Madingley Road, Cambridge CB3 OHA, England; schwarz@ast.cam.ac.uk
AND
M. E. MANDY
Programme in Chemistry, University of Northern British Columbia, Prince George, BC V2N 4Z9, Canada; mandy@unbc.edu
Received 1995 May 30; accepted 1995 October 20

ABSTRACT

The master equation for collisional excitation of H_2 by H atoms is solved over a temperature range of $T = 450$–$45{,}000$ K and a density range of $n_H = 10^{-3}$–10^9 cm^{-3}. Radiative transitions due to quadrupole emission and dissociative tunneling are included explicitly. The resulting nonequilibrium steady state populations of the (v, j) states of H_2 are determined and then used to calculate the rate coefficients for ortho-para interconversion, collisional dissociation, dissociative tunneling, and cooling. The density and temperature dependences of these rates are discussed and parameterized. Comparisons with previous estimates are made.

Subject headings: ISM: molecules — line: formation — molecular data — molecular processes

1. INTRODUCTION

Evaluation of several fundamental processes involving H_2 requires a detailed knowledge of the populations of the vibration-rotation $[(v, j)]$ states of the molecule; prominent among these are prediction of the quadrupole emission spectrum, radiative and dissociative cooling in the relaxation of an interstellar shock (see, e.g., Hollenbach & McKee 1989), and heating by "quenching" of H_2 that is fluorescently excited in photodissociation regions (see, e.g., Sternberg & Dalgarno 1989). Since the interstellar medium is not generally in local thermodynamic equilibrium, the relative populations of the (v, j) states of molecular H_2 cannot be described adequately with the Boltzmann distribution. Instead, the competing processes that can affect the population such as radiative emission and absorption, and collisional excitation, deexcitation, and dissociation must be treated explicitly. The equation that describes the evolution of state populations is often called the master equation (§ 2).

In this paper we use a new set of rate coefficients for collisions of H_2 with H, describing both state-to-state transitions and collision-induced dissociation (CID; Mandy & Martin 1993, 1996). The significant differences in these rate coefficients with respect to earlier estimates based on various more approximate calculations have been discussed by Mandy & Martin (1993), pointing to a need for revised cooling and CID rates. A novel feature of the new rate coefficients is that the set is complete; examination of the complete results has called into question the assumption that only a few types of collisional transitions are important (Mandy & Martin 1993). Therefore, in our master equation calculations no restriction has been placed on the number of (v, j) states or on the types of collisional transitions connecting them.

The calculations reported here, and their earlier counterparts, are based on finding steady state populations at a particular temperature and density. Solution of the master equation is also an integral part of simulations of more complex situations where the populations and physical conditions are changing in time and/or space (e.g., interstellar shocks and photodissociation regions), in which case the steady state populations for the local temperature and density sometimes might not be achieved (Lepp & Shull 1983; Chang & Martin 1991). In any case, incorporation of the new rate coefficients directly into such calculations should bring quantitative improvement, and the steady state solutions at particular temperatures and densities will provide useful insight into more complex situations.

In § 2 we discuss the details of our master equation calculation, the data used in its implementation, and the numerical method used to solve this stiff set of equations. From fractional populations on a grid of varying density and temperature, rate coefficients for ortho-para interconversion, dissociation, and cooling are calculated, with a focus on how they depend on density and temperature (§ 3). Analytic expressions encapsulating these dependences are summarized in the Appendix. In § 4 we conclude with a discussion that includes comparisons to earlier rate coefficient estimates and, where possible, to laboratory experiments.

2. IMPLEMENTING THE MASTER EQUATION

The master equation provides the means to determine the populations of all the (v, j) states of H_2 by considering explicitly all processes of interest that can populate and depopulate these states. While, in theory, it is possible to include all processes that can affect the population of the states, in practice only selected ones are included. In this study we consider radiative deexcitation by quadrupole emission, dissociative tunneling, and the collisional processes of excitation, deexcitation, and dissociation. This allows a straightforward comparison with the results of earlier studies (Lepp & Shull 1983; Roberge & Dalgarno 1982; Dalgarno & Roberge 1979; Hollenbach & McKee 1979) to assess the effects of the new rate coefficients and inclusion of all transitions among the (v, j) states.

For the collisional processes, we consider only H atoms

as collision partners, corresponding to dilute H_2 in a bath of H atoms. Interstellar formation of H_2 occurs on grain surfaces, with rate coefficient $\sim 10^{-17}$ cm^3 s^{-1} over a range of gas temperatures (Hollenbach & McKee 1979; Sternberg & Dalgarno 1989, 1995); simple two- and three-body recombination is much slower. For the interstellar warm gas conditions in which we are interested H_2 would not be *infinitely* dilute, and we find that the fractional change in the amount of H_2 caused by recombination would be small on the timescale in which steady state fractional populations of the (v, j) states are established. We have ignored recombination. Nevertheless, as discussed in § 3, it is possible that inclusion of recombination might alter both the relative populations of highly excited (v, j) states and any derived bulk quantities that are sensitive to these populations.

Since interstellar H_2 would normally be optically thin in quadrupole lines, we have excluded reabsorption of the quadrupole emission. We have also excluded ultraviolet fluorescent pumping, a fundamental process in photodissociation regions (Tielens & Hollenbach 1985; Sternberg & Dalgarno 1989). The influence of recombination and fluorescent pumping on the rotational excitation seen via ultraviolet absorption measurements in *cold* interstellar gas is an interesting problem (see, e.g., Wagenblast & Hartquist 1989) beyond the scope of this paper.

The present calculations have relevance in assessing the conditions in clouds in which H_2 is not the predominant form of neutral hydrogen, including some chemistry in the early universe (see, e.g., Shapiro 1992). There are situations in which it would be desirable to consider other collision partners for H_2, especially another H_2. This would permit an assessment of the chemistry of molecular clouds in which H_2 is the dominant species. Chemical reaction networks are sensitive to the fractional abundances of H, H_2, and H^+ and hence to the extent of dissociation of H_2. In the case of internal energy transfer being studied here, the behavior with collision partner H_2 is expected to differ significantly from that with H. A collision with atomic H with its open electronic shell is more likely to promote large changes in (v, j) in the H_2 target molecule than is a collision with the closed shell H_2 molecule. Also the barrier to exchange is much lower. Thus, it is anticipated that even when H_2 is not infinitely dilute in H atoms and $H_2 + H_2$ collisions have to be considered, $H + H_2$ collisions might still dominate important aspects of the overall kinetics.

In our model all 348 (v, j) states of H_2 in its electronic ground state are included. As displayed in Figure 1, these consist of manifolds of j states for $v = 0$ to 14. Within each manifold, quantum numbers j can range from 0 to j_{max}, with the actual value of j_{max} depending on the value of v ($j_{max} = 38$ for $v = 0$, $j_{max} = 4$ for $v = 14$). These states include 47 that are "quasi-bound" (Blais & Truhlar 1979). A quasi-bound diatomic molecule has an internal energy in excess of what is required for dissociation; see, e.g., (0, 32) in Figure 1. It is confined for a finite lifetime in this state by the rotational barrier, through which tunneling can occur, leading to spontaneous dissociation. When this lifetime is less than the collision time, this phenomenon is sometimes referred to as rotational predissociation. Dissociative tunneling from the quasi-bound states can make a significant contribution to the total dissociation rate, especially in low-density regimes where the collisions times are large. The tunneling probability (§ 2.2) varies strongly with the (v, j) state and can be quite large, further increasing the stiffness of the master equation and posing special challenges in numerical modeling.

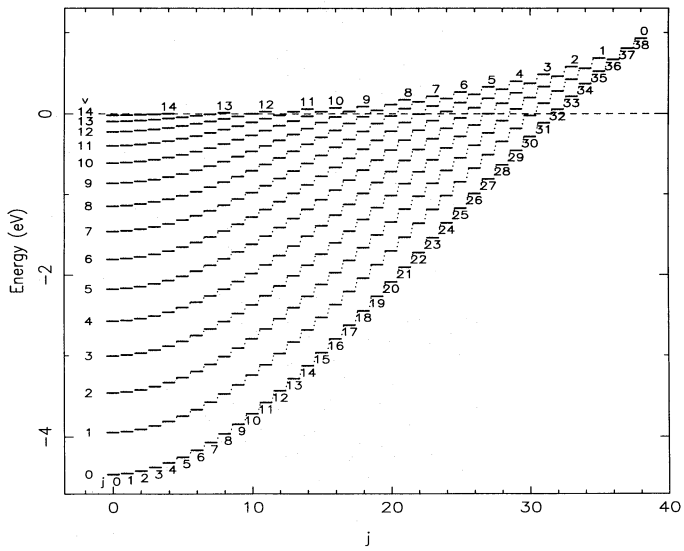

FIG. 1.—(v, j) energy levels of the H_2 molecule in its ground electronic state. The dissociation energy is indicated by the dashed line.

Let n_k be the population of a (v, j) state with energy E_k. The sum of these populations is n_{H_2} and the fractional population $p_k = n_k/n_{H_2}$. Let n_{349} represent the population that has become unbound (because H_2 is assumed to be infinitely dilute in H, $2n_{349}$ does not modify the H atom density n_H). For the bound states, the master equation for our restricted problem then has the form

$$\frac{dn_k}{dt} = \sum_{l:E_l>E_k} A_{kl} n_l - \sum_{l:E_k>E_l} A_{lk} n_k + n_H \sum_{l\neq k} (\gamma_{kl} n_l - \gamma_{lk} n_k) - r_{349,k} n_k , \quad (1)$$

where we adopt the matrix-motivated convention that subscript kl represents a transition *to* state k *from* state l (i.e., $kl \equiv k \leftarrow l$). A_{kl} is a radiative transition probability (§ 2.3), γ_{kl} is a collisional rate coefficient (§ 2.1), and $r_{349,k}$ is a dissociative tunneling transition probability (zero except for the quasi-bound states; § 2.2). The availability of electronic versions of these data is described in Appendix C.

Equation (1) is supplemented by

$$\frac{dn_{349}}{dt} = \sum_{l=1,348} (n_H \gamma_{349,l} + r_{349,l}) n_l . \quad (2)$$

This coupled set of 349 equations can be expressed readily in the matrix form required by the numerical method for solution. We wish to integrate the master equation to a steady state, that is, until the rates of change of the fractional populations of the (v, j) states are (close to) zero:

$$dp_k/dt \simeq 0 . \quad (3)$$

Note that as temperature and density increase, dn_{H_2}/dt (given by the negative of eq. [2]) increasingly departs from zero; in this study this leads to a significant depletion of the molecules at the highest temperature and density conditions considered (§ 2.4).

2.1. *Collisional Rate Coefficients*

The only collisional processes considered in this study are those of molecular H_2 interacting with H atoms. The interaction potential energy surface for $H + H_2$ is well known for the ground electronic state (Liu 1973; Siegbahn & Liu 1978; Truhlar & Horowitz 1978; Varandas et al. 1987;

Boothroyd et al. 1991, 1996). The rate coefficients γ used here were determined from cross sections that had been calculated with the quasi-classical trajectory (QCT) method using the LSTH potential energy surface (see Mandy & Martin 1993 and references therein for details). Limited comparisons of various revised surfaces and (low-energy) cross sections based on them indicate that the LSTH calculations should be quite accurate (Mandy & Martin 1991, 1992; Keogh et al. 1992; Sun & Dalgarno 1994; Lepp, Buch, & Dalgarno 1995; Boothroyd et al. 1996).

Outcomes of $H + H_2$ collisions fall into three classes: nonreactive, in which an inelastic collision leaves the original H_2 molecule in a different (v, j) state, which must be of the same nuclear spin parity; exchange, in which the atomic H collision partner combines with one of the H atoms of the target diatomic to form an new H_2 molecule in some (v, j) state (among such collisions are those that change the parity, which we refer to as ortho-para interconversion); and dissociation, in which the molecular bond is severed leaving three H atoms. All of these processes are included here. Rate coefficients have been evaluated at 15 temperatures between 450 and 45,000 K (about 180,000 coefficients per temperature, 120,000 exchange plus 60,000 nonreactive, which were evaluated separately in the QCT method).

Some caution must be exercised in using the rate coefficients at the high end of this temperature range. Although most excited electronic state potential energy surfaces for $H + H_2$ are well separated from the ground electronic state potential energy surface considered here, there is one that has a conical intersection with the ground state surface for D_{3h} geometries, the lowest of which is at 2.7 eV, about $\frac{2}{3}$ of the way to the dissociation limit (see Fig. 1). The possibility that collisions are not electronically adiabatic is expected to affect collisional cross sections at high energy, and hence rate coefficients at higher temperatures, above $\sim 10^4$ K. While this has not been explored in any detail, available information suggests that the effect will be less than 50% for state-to-state transitions (Blais, Truhlar, & Mead 1988; D. Truhlar 1991, private communication). Wu & Kuppermann (1993) have shown that quantum interference related to the conical intersection can have a measurable (and oscillating) effect on the cross section at total energies as low as 1.8 eV. Although the net effect on nonreactive or reactive rate coefficients has not been assessed quantitatively it is unlikely to be large at the temperatures in which we are interested (A. Kuppermann 1995, private communication).

There are other unmodeled complications that could arise in a high-temperature gas, including electronic excitation of the H collision partner, and increasing fractional ionization in the ambient gas, which would introduce electrons and protons as other collision partners. It can also be noted that at high temperatures collisional dissociation is rapid and H_2 is short-lived. When we carried out calculations at 45,000 K, we found H_2 largely destroyed by the time steady state populations were achieved (§ 2.4). Furthermore, because of rapid dissociative cooling, a simulation at a constant high temperature might not be relevant in many astrophysical applications.

Caution must also be exercised at the low end of the temperature range because the rate coefficients become increasingly sensitive to the energy dependence of the cross section near threshold. The statistical noise in the QCT cross sections is largest when the cross sections are small (as they usually are near the threshold for a transition). Also the QCT approach, by its very nature, does not include quantum effects that are expected to become increasingly important at lower T. To gauge the magnitude of this effect, where available the quantum cross sections for reactive transitions between (0, 0) and a few of the lower energy (v, j) states were substituted in the calculation of the rate coefficients (Mandy & Martin 1993). At 1000 K the changes in the values of the rate coefficients caused by the substitution of the quantum results amounted to 25% rms and 53% maximum; at 10,000 K these decreased to 8% and 14%, respectively. As mentioned, master equation solutions were obtained for T as low as 450 K.

For physically meaningful results from the master equation, the collisional rate coefficients used must obey detailed balance (microscopic reversibility; Mandy & Martin 1993) to numerical accuracy. Calculating the upward coefficient γ_{lk} $(E_l > E_k)$ to machine accuracy from the downward coefficient γ_{kl} using detailed balance ensures that this is the case.

2.2. *Dissociative Tunneling*

The (v, j) states that are quasi-bound (or rotationally predissociated) have a finite probability of tunneling through the rotational barrier to form an unbound dissociated state. The dissociative tunneling transition probabilities have been found from

$$r_{349,k} = 2\pi c \Gamma_k , \tag{4}$$

where Γ_k is the energy width of state k (measured here in cm^{-1}) as calculated by LeRoy & Bernstein (1971) and Schwartz & LeRoy (1987).

It is possible to classify the quasi-bound (v, j) states into two broad groups based on the magnitude of the dissociative tunneling transition probability relative to that for radiative deexcitation or collision. For most quasi-bound states, dissociative tunneling is the most probable of the processes unless the density is very high (we have included the collisional $[\gamma_{kl}]$ coefficients in the calculation for all quasi-bound states, although their role is significant only at higher densities). In the interstellar medium and in some laboratory conditions, a molecule excited to one of these (v, j) states is effectively dissociated.

The second group is composed of the few states with high j and internal energies only slightly above the dissociation energy. These states have much smaller tunneling transition probabilities that are comparable to or smaller than the Einstein A-values and much smaller than the probability of collisional energy transfer at the densities of interest, and so to avoid an artificial buildup of their populations it is necessary to treat them in the same manner as the classically bound states by including their radiative transition probabilities (see § 2.3). The six (v, j) states so treated were (0, 32), (0, 33), (1, 31), (2, 29), (4, 26), and (5, 24).

2.3. *Radiative Transitions*

Radiative emission from a (v, j) state of H_2 obeys the quadrupole selection rule: $\Delta j = 0, \pm 2$, except in the case of $j = 0$, where only $\Delta j = 2$ is allowed. Thus, radiative transitions cannot lead to ortho-para interconversion. There is no restriction on the change in vibrational quantum number save through the requirement that the energy of the final state be below that of the emitting state. We used the A_{kl} of Turner, Kirby-Docken, & Dalgarno (1977), supple-

mented for some higher states by further calculations (A. Dalgarno 1982, private communication). Values were required for several (v, j) states with internal energy close to the dissociation limit, namely (0, 31), (3, 27), and the six boundlike quasi-bound states mentioned above (§ 2.2). Their A_{kl}-values were extrapolated from adjacent smoothly behaved values.

2.4. *Numerical Solution*

This system of first-order differential equations is stiff in that the transition probabilities involved span many orders of magnitude as do the populations of the (v, j) states. The routine D02EJF in the NAG Fortran Library (Fox & Wilkinson 1990) provides an appropriate method to solve this system of equations. This routine uses a variable-order, variable-step method implementing the backward differentiation formulae. The starting conditions are unimportant to the steady state result. In practice, we initialized the populations to the corresponding Boltzmann populations if both $n_H > 100$ cm^{-3} and $T > 10{,}000$ K; otherwise we populated only the lowest ortho and para states at 0.75 and 0.25, respectively. The integration proceeds until a user-specified function of the solution is zero. The function we used takes the maximum of the fractional changes in the non–quasi-bound populations after each time step and divides it by the time step (see eq. [3]). A steady state is deemed to have been reached when this maximum is below some specified value and the integration is terminated. Sensitivity tests showed that by using this criterion, and for the integration tolerances chosen, the steady state populations of the states could normally be determined to better than four significant figures.

However, at higher temperatures and densities it was necessary to adopt another criterion to stop the integration. Under these physical conditions the probability of dissociation of H_2 was sufficiently high that our solution without recombination could approach $p_{349} = 1$ without the above precise termination criterion being met; negative values for the populations of some of the 348 states could then occur as numerical artifacts. Instead, the integration was stopped when 99% of the initial H_2 had dissociated. For the range (grid) of physical conditions studied (§ 2.4.1), this affected only the 45,000 K model at $n_H = 10$ cm^{-3}, those for $T \geq 20{,}000$ K at $n_H = 10^3$ cm^{-3} and those for $T \geq 10{,}000$ K at $n_H \geq 10^6$ cm^{-3}. In these cases the solutions were examined to assess how closely they appeared to be approximating steady state conditions and it was found that the fractional populations were converged to better than 0.5%.

Since the steady state populations of the excited states for all models were determined to better than 0.5%, the cooling, dissociation and ortho-para interconversion rates that were calculated directly from these populations have similar (or better) accuracy. Thus, our solution of the master equation did not add significantly to the uncertainties already implicit in the calculation due to the uncertainties in the collisional rate coefficients, the dissociative tunneling probabilities, or the radiative emission probabilities.

The large values of some of the dissociative tunneling probabilities contributed significantly to the stiffness of the system. To facilitate the numerical solution it was possible to cap their values at a factor 10^6 times larger than the greater of the A-value or the collisional probability (at that density) and still not affect significantly the solution. A consequence is that the quasi-bound states with large (true) values of the probability for dissociative tunneling are overpopulated relative to the true steady state solutions. The dissociative tunneling rate is the product of the smaller adopted coefficients and the artificially larger populations of the quasi-bound states. Thus, we were able to reproduce the true rate in our calculations; in each of the test cases we considered agreement was significantly better than the 0.5% from our worst-case convergence. Radiative cooling or CID from these overpopulated states was insufficient to affect populations of other states; since the affected quasi-bound states are still underpopulated relative to the other excited states, there is no detrimental effect on the assessment of cooling or dissociation from the whole system (contributions to these global quantities are again much less than 0.5%).

2.4.1. *Range of Physical Conditions*

The range of physical conditions that can be considered is constrained by the validity of the collisional rate coefficients (450–45,000 K; see § 2.1) and, practically, by whether the solution of the master equation converges to a steady state. Both of these factors serve to restrict the temperature range, but are compatible. We found that below 450 K a steady state could not be attained within a reasonable amount of computer time. Above 45,000 K solutions indicate that the molecular dissociation is virtually complete before the fractional populations of the (v, j) states come to within 0.5% of the steady state.

The range of densities was chosen to be $n_H = 10^{-3}$–10^9 cm^{-3}. We found that this range adequately spanned the regime where we wished to assess the competing effects of collisional processes and radiative decay. Outside this range, steady state populations did not change significantly with density (unless the density becomes extremely high, $\approx 10^{20}$ cm^{-3} and greater; there the collisional rates become comparable to the rate of dissociative tunneling, and there is again a strong dependence of populations on the density).

3. RESULTS

Steady state populations were found for a grid of physical conditions: 15 temperatures from 450 K to 45,000 K (450, 600, 780, 1000, 1400, 2000, 3000, 4500, etc.), and 13 densities spanning the range $n_H = 10^{-3}$–10^9 cm^{-3} at order-of-magnitude intervals. A selection of the results from the total of 195 simulations will be presented, making use of graphical displays to support our qualitative interpretation and discussion. The fundamental data are the population distributions that are described in the first subsection. We are also especially interested in such bulk quantities as the rates of dissociation, cooling, and ortho-para interconversion. These are calculated once the populations are determined. Observing how the population distribution changes with density and temperature is essential to understanding the behavior of the bulk quantities. To provide quantitative results, these rates have been parameterized using interpolating functions of temperature and density (see Appendix).

3.1. *The Populations*

Figure 2 shows the energy levels of Figure 1 contoured as functions of v and j. This basic behavior serves as background and orientation for the displays of (v, j) population distributions, which will be contoured in similar diagrams. States to the lower left are more tightly bound and so will

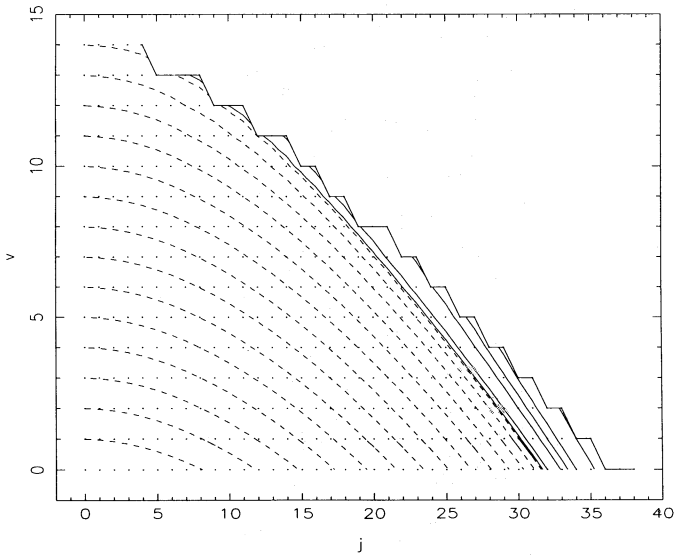

FIG. 2.—(v, j) energy levels of the H_2 molecule contoured as functions of v and j. Negative energies (bound states) are represented by the dashed lines; the 14 contours correspond to the energies of 14 excited $(v, 0)$ states. The first solid contour corresponds to the dissociation energy. The other solid contours are for positive energies for a few of the many quasi-bound states: (0, 32), (2, 30), (1, 32), (0, 34), (1, 34).

have larger populations. Because of the roughly three to one ratio of ortho to para hydrogen (§ 3.2), it is necessary to plot their distributions separately, but other than this scaling they are very similar in shape.

At high density, where collisional energy transfer is the dominant process, the populations are closest to the Boltzmann distribution. This is illustrated in Figure 3*a* for the steady state at $T = 2000$ K and $n_H = 10^9$ cm^{-3}. The contours of the distribution roughly parallel the energy contours (Fig. 2), except at low j where the states have low statistical weight. However, the distribution is not quite Boltzmann. As a result of dissociative tunneling, most quasi-bound states are highly depleted; note the normal behavior of the ortho boundlike quasi-bound states (0, 33), (1, 31), and (2, 29), which have low tunneling rates. Furthermore, CID depletes, less dramatically, those bound states near the dissociation limit, especially at high v and low j, where the CID rate coefficients are largest (see below). Note that in our simulations neither mode of depletion is compensated by recombination. Because these relative (fractional) populations within H_2 sum to unity there is a corresponding slight overpopulation of the lowest energy (v, j) states; this is most pronounced at high temperature. A consequence of the underpopulation of the highest states is that the average internal vibrational-rotational energy of the H_2 is also less than the thermal equilibrium value kT for each mode. The rotational mode can be substantially excited toward this thermal equilibrium value by 1000 K, but the vibrational mode is never fully excited, even at the higher values of T (see also Chang & Martin 1991, Fig. 6).

At low density, where the probability of collision is sufficiently low that radiative emission is the dominant process, any collisionally excited H_2 molecule is likely to lose all internal energy (in excess of the zero point energy) by a radiative cascade before undergoing another collision. Thus, the populations are far from Boltzmann, mostly occupying the two ground (v, j) states (0, 0) and (0, 1). In the slightly excited (v, j) states there are *trace populations that scale linearly with density*; the range of these excited states becomes more extensive at higher temperatures.

At densities intermediate between these extremes, there is a competition between radiative deexcitation and collisional redistribution. Figure 3*b* shows the population distribution for $T = 2000$ K and $n_H = 10^3$ cm^{-3}. It has the same characteristic shape as Figure 3*a*, but the excited-state populations are very much depressed (hence the contours are more closely spaced). For example the contours 10^{-4} and 10^{-9} of Figure 3*a* more or less overlie the contours 10^{-6} and 10^{-12} in Figure 3*b*. Comparison of the horizontal spacing of the contours at fixed v in Figure 3*b* relative to

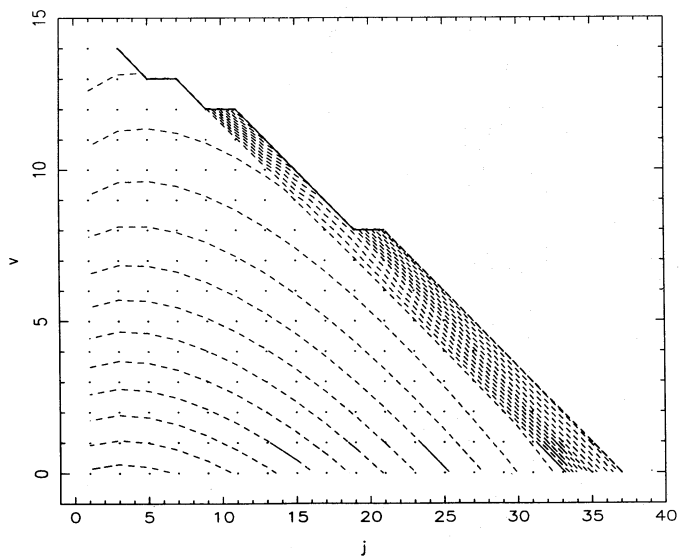

FIG. 3*a*

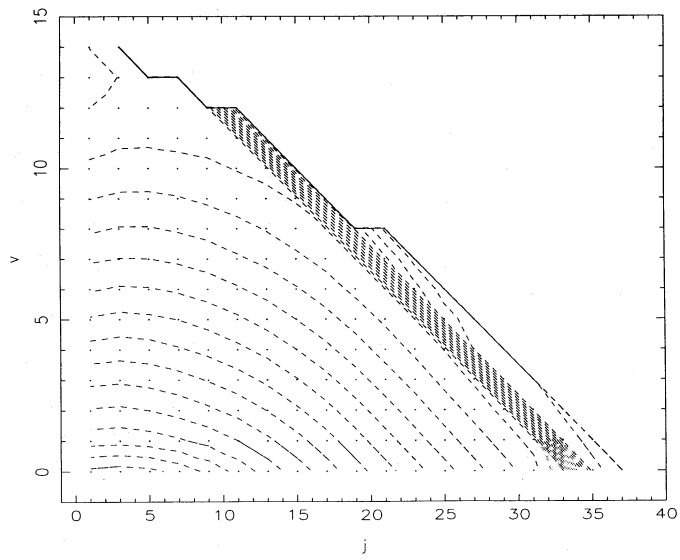

FIG. 3*b*

FIG. 3.—(*a*) Contour plot of the steady state fractional populations of (v, j) states of H_2 at $T = 2000$ K and $n_H = 10^9$ cm^{-3}. Contours are at 1 dex intervals, decreasing from a value 10^{-1} in the lower left. Steep falloff in populations near the dissociation limit arises from collision-induced dissociation and, for quasi-bound states, from dissociative tunneling as well. (*b*) Same as (*a*), but for $n_H = 10^3$ cm^{-3}. The effect of the cap on the tunneling rate (§ 2.4) can be seen in the overpopulations of the highest energy quasi-bound states.

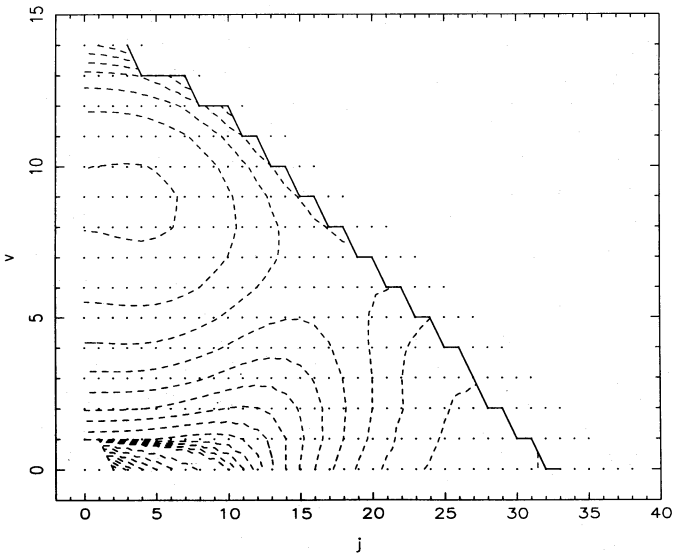

FIG. 4*a*

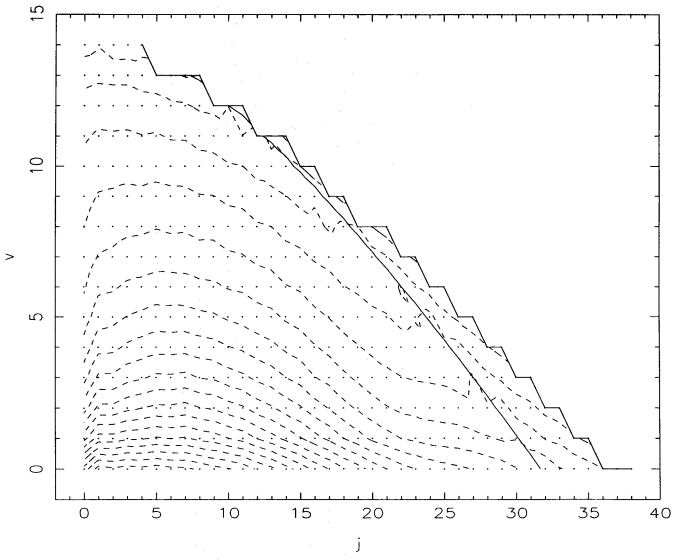

FIG. 4*b*

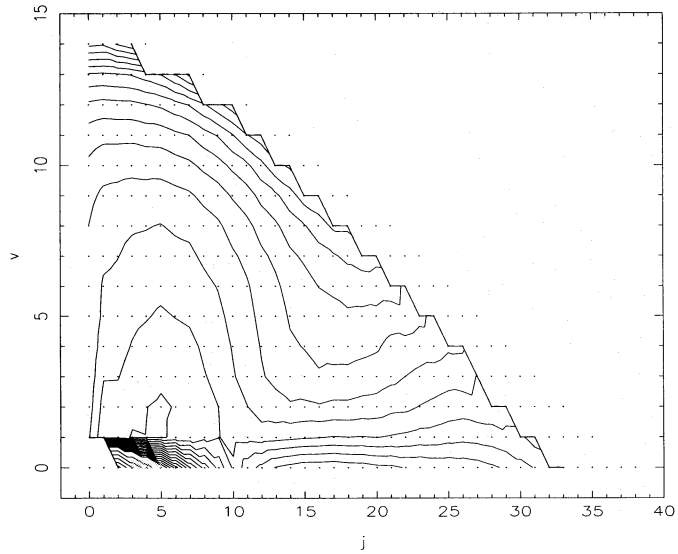

FIG. 4*c*

FIG. 4.—(*a*) Contour plot of the probabilities of (v, j) states depopulating by quadrupole radiative emission. The first set of 13 contours are at 0.1 dex intervals, decreasing from a value 5×10^{-6} s^{-1} for the contour encircling the maximum at (0, 27) and the local maximum at (9, 3) [the contour passing near (5, 15) dividing these two maxima is at a value 2.5×10^{-6} s^{-1}]. Thereafter, in the lower left as the probabilities continue to decrease, at contour level -6.5 dex the contour interval increases to 0.5 dex. (*b*) Contour plot of the rate coefficient for (v, j) states depopulating by collisional energy transfer and dissociation at $T = 2000$ K. Contours are at 0.1 dex intervals increasing from a value 5×10^{-11} cm^3 s^{-1} at the lower left to 3.2×10^{-9} cm^3 s^{-1} at the upper left. (*c*) Contour plot of critical density of (v, j) states at $T = 2000$ K, formed from the ratio of the values in (*a*) and (*b*) (eq. [5]). The first 14 contours are at 0.1 dex intervals decreasing away from a value 6.3×10^3 cm^{-3} for the closed contour around (2, 5). Subsequently, in the lower left at contour level 2.5 dex the contour interval increases to 0.5 dex. Along $v = 0$ the critical density rises rapidly from a value 6.2×10^{-1} cm^{-3} for (0, 2) to a maximum of 1.2×10^4 cm^{-3} for (0, 17).

Figure 3*a* shows that the ratios of populations within a given v manifold are not generally equal to the Boltzmann ratios (Lepp & Shull 1983); particularly for the higher j states, which are at increasingly higher energies (Fig. 1), the populations are relatively depressed.

Figure 4 illustrates how there is a (temperature-dependent) "critical density" $n_{\mathrm{H},k}$ for each particular (v, j) state k, at which the probability of depopulation by radiative emission (Fig. 4*a*; no T dependence) is equalled by that from collisional energy transfer (combined rate coefficients contoured in Fig. 4*b* for 2000 K):

$$n_{\mathrm{H},k} \sum_{l=1,349} \gamma_{lk} = \sum_{l:E_k>E_l} A_{lk} \,, \qquad (5)$$

(or more compactly $n_{\mathrm{H},k}\Gamma_k = A_k$). Thus, the ratio of the values in Figures 4*a* (A_k) and 4*b* (Γ_k) gives the critical density shown in Figure 4*c* (we ignore dissociative tunneling for the quasi-bound states). In the derived (bulk) quantities to be discussed below, behavior related to critical density is exhibited as a region of sharp change in the dependence on density. Since individual states have different critical densities, and since the population distributions (as well as the critical densities) depend on temperature, the position and sharpness of this transition from low- to high-density asymptotic behavior exhibits temperature dependence.

The uncertain contribution of recombination to the excitation of H_2 is often excluded (see, e.g., Burton, Hollenbach, & Tielens 1990), as we have done here. The process of H_2 formation on grain surfaces is subject to considerable uncertainty (Sternberg & Dalgarno 1989, 1995), with the rate coefficient estimated to be $R \sim 10^{-17}$ cm^3 s^{-1} for the conditions of interest here. While the newly recombined H_2 will be internally excited, various conflicting suggestions have been made as to the details of this excitation distribution. For example, Sternberg & Dalgarno (1989) adopt the simple assumptions made by Black & Dalgarno (1976) that there is equipartition with one-third of the binding energy available for H_2 internal excitation and that this energy is statistically distributed. With these assumptions, the branching coefficients β_k into state k follow a Boltzmann distribution at about 17,000 K; for (ortho) states within about 1 eV of the dissociation limit $\beta_k \sim 3 \times 10^{-3}$ (relatively higher for high j at the same energy) leading to entry rate coefficients $R\beta_k \sim 3 \times 10^{-20}$ cm^3 s^{-1}. On the other hand, Wagenblast & Hartquist (1989) adopt a model advanced by Duley & Williams (1986) in which there is very little rotational excitation (j is 0 or 1) and v is intermediate (~ 7); these states are about 1.5 eV or more below the dissociation limit (Fig. 1) and might have β_k as large as 10^{-1}.

Clearly, there is a lot of parameter space to explore to see what effects might arise. This is beyond the scope of this paper, but we can make an estimate to illustrate the potential importance.

The rate coefficient due to recombination, $R\beta_k$, which affects dn_k/dt can be compared directly to the exit rate coefficient from state k due to collisions and radiative emission, $(n_{H_2}/n_H)p_k(\Gamma_k + A_k/n_H)$, which for steady state values of p_k balances the entry rate coefficient. Consider states about 1 eV below the dissociation limit, for which $A_k \sim 3 \times 10^{-6}$ s^{-1} (Fig. 4*a*) and $\Gamma_k \sim 10^{-9}$ cm^3 s^{-1} at 2000 K (Fig. 4*b*). Above the critical density ($\sim 3 \times 10^3$ cm^{-3}; Fig. 4*c*), $p_k \sim 10^{-9}$ (Fig. 3*a*). In the case used by Sternberg & Dalgarno, we then compare $R\beta_k \sim 3 \times 10^{-20}$ cm^3 s^{-1} to $10^{-18}(n_{H_2}/n_H)$ cm^3 s^{-1}, indicating that recombination contributions would be competitive if $(n_{H_2}/n_H) < 3 \times 10^{-2}$. At lower densities like 10^3 cm^{-3}, A_k comes into play, p_k becomes smaller ($\sim 10^{-12}$ in Fig. 3*b*) and the limit on (n_{H_2}/n_H) rises somewhat (note that $A_k p_k/n_{H_2}$ stabilizes at low densities).

Qualititatively, the states likely to be most affected are those with the lowest populations (high-energy states, low-temperature and/or low-density conditions); their total population would be negligible compared to the population of lower energy states. Thus, we expect that only those quantities that depend sensitively on the populations of these highly excited states might be affected by recombination. These would include line emission from these states (not addressed here) and dissociation (§§ 3.3 and 4.2), but not ortho-para interconversion (§ 3.2) or radiative cooling (§ 3.4).

There are of course other complications that could be considered too. When recombination is in a steady state with ultraviolet photodestruction of H_2, the accompanying fluorescent excitation of molecules escaping photodestruction can also affect the populations of the high-lying energy states. In a plasma, production of excited H_2 by associative detachment of $H + H^-$ might become interesting too (Black, Porter, & Dalgarno 1981). Thus, model assumptions should be examined critically before the results are widely applied: *caveat emptor*.

3.2. *Ortho-Para Interconversion*

Nuclear spin considerations determine whether a molecule of H_2 is in an ortho or para state. Para H_2 has antiparallel nuclear spins, which restricts the rotational quantum number j to even values. Parallel nuclear spins are characteristic of ortho H_2 with odd values of j. These states have statistical weight $g = (2s + 1)(2j + 1)$, where the nuclear spin factor s is 0 for para and 1 ortho. In our modeling of H_2 infinitely dilute in H, ortho-para interconversion occurs only as the result of the exchange reaction. Quadrupole emission and nonreactive energy transfer do not change the nuclear spin and thus can change j by only even values.

The rate coefficient for exchange from ortho to para hydrogen, γ_{po}, is simply obtained:

$$\gamma_{po} = \sum_{k:\text{ortho}} \sum_{l:\text{para}} \gamma_{lk} p_k \,. \tag{6}$$

A similar equation holds for para to ortho conversion and for steady state populations $\gamma_{po} = \gamma_{op}$. Independent evaluation of the two rate coefficients (including for Boltzmann populations) provides useful numerical checks. In Figure 5 we show loci of γ_{po} as a function of density n_H for fixed values of temperature T. Changes in the bulk quantity γ_{po} reflect changes in the steady state populations for the different physical conditions. The timescale for conversion is $1/(\gamma_{po} n_H)$. We found that these population-weighted values were dominated by the contributions from the lower (v, j) states; furthermore, there is only a small change as the populations change over a wide range. Because recombination affects primarily the populations of the upper states, we expect the exclusion of this process from our model not to affect this bulk rate coefficient for ortho-para conversion.

In the low-density limit, any collisional excitation (or exchange) is followed by radiative emission, which does not contribute (further) to the exchange reaction. The conversion rate coefficients γ_{op} and γ_{po} are simply the sums of the state-to-state exchange rates from (0, 0) and (0, 1), respectively (see eq. [7]). Classically a total energy of 0.424 eV (0.155 eV relative to the zero point) is the minimum required for exchange, although quantum mechanically tunneling though this barrier can occur. This energetic barrier is reflected in the steep temperature dependence at lower temperatures. The temperature dependence weakens at higher temperatures as transitions to higher energy states become accessible.

At higher densities excited states can be significantly populated (depending on T) and so come into play in the conversion rate coefficient. The rate coefficients from the excited states tend to be higher with increasing energy of the state, accounting for the increase in γ_{po} with density (at a given T). This is most pronounced for higher temperatures where the excited-state populations become most significant. However, the higher density γ_{po}'s are not monotonic with temperature above 14,000 K because of the increased importance of dissociation from the excited states near the dissociation limit that depletes their populations. For the same reason, these high-density ($n_H = 10^9$ cm^{-3}) "limiting" rate coefficients are depressed relative to those obtained assuming Boltzmann populations.

3.2.1. *The Density Dependence of the Ortho to Para Ratio*

In Figure 6 we consider the ratio of the population of ortho states to that of para states. If thermal equilibrium were reached (at least for the states most relevant to the conversion), then at high temperatures (many excited states accessible) a ratio near 3 would be expected on the basis of nuclear spin considerations. For Boltzmann populations at or above 450 K, this is indeed the case, and this ratio is approached in our high-density limiting cases too. At lower temperatures, the ratio decreases because of the diminishing Boltzmann factor for state (0, 1) with respect to (0, 0) in the partition function (the energy difference corresponds to 170.5 K).

As the density decreases, the populations deviate further from the Boltzmann distribution and in the limit only states (0, 0) and (0, 1) are populated. This limit is reached by $n_H = 10^{-3}$ cm^{-3} except for the highest temperatures in our grid; at 45,000 K $p_{(0,2)} = 1 \times 10^{-2}$ and $p_{(0,3)} = 2 \times 10^{-3}$. Without going through the full master equation numerical solution (and hence as a check), the fractional populations of the two ground states in this limit are determined by solving

$$\sum_{k:\text{ortho}} \gamma_{k,(0,0)} p_{(0,0)} = \sum_{k:\text{para}} \gamma_{k,(0,1)} p_{(0,1)}$$

$$\text{and} \quad p_{(0,0)} + p_{(0,1)} = 1 \,. \tag{7}$$

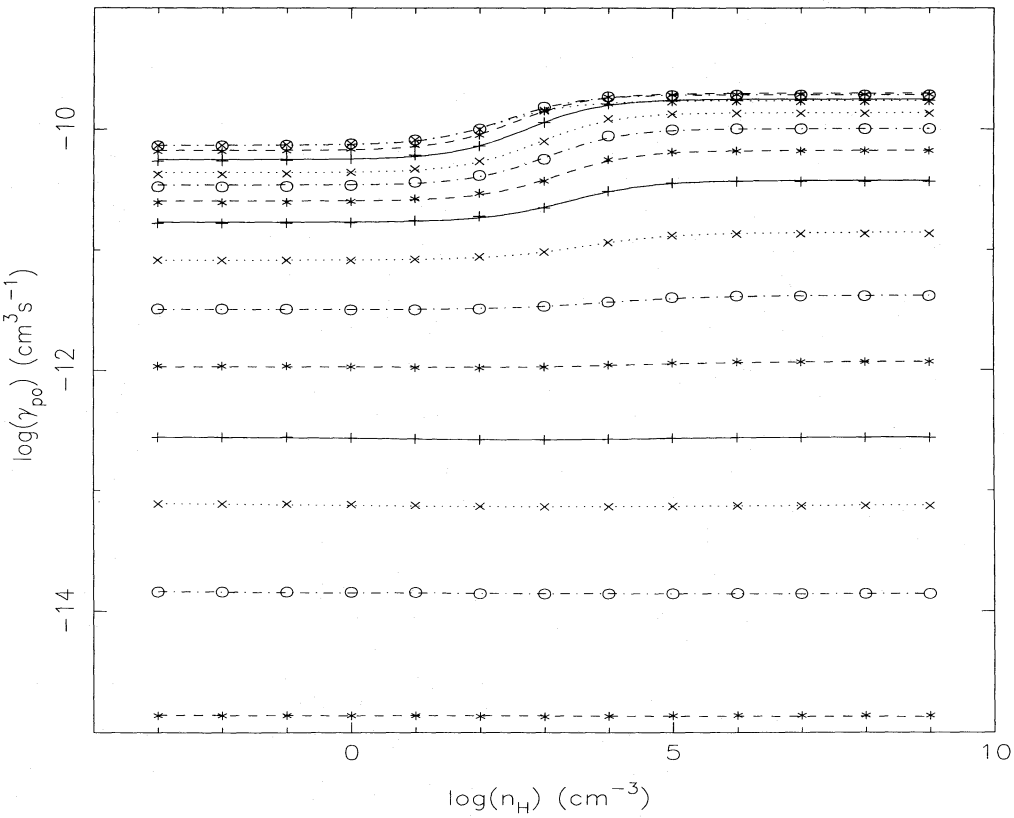

FIG. 5.—Steady state rate coefficient γ_{po} for conversion of ortho to para H_2 (and vice versa) as a function of collision partner density n_H. Values for constant T are joined by curves whose analytic form is given in the Appendix. Beginning at the lower part of the diagram, the 15 values in the T grid are 450 K, 600 K, 780 K, 1000 K, 1400 K, 2000 K, 3000 K, 4500 K, 6000 K, 7800 K, 10,000 K, 14,000 K, 20,000 K, 30,000 K, and 45,000 K; the systematic order of different line types (and symbols) helps in deciphering T in the upper part of the diagram where lines overlap.

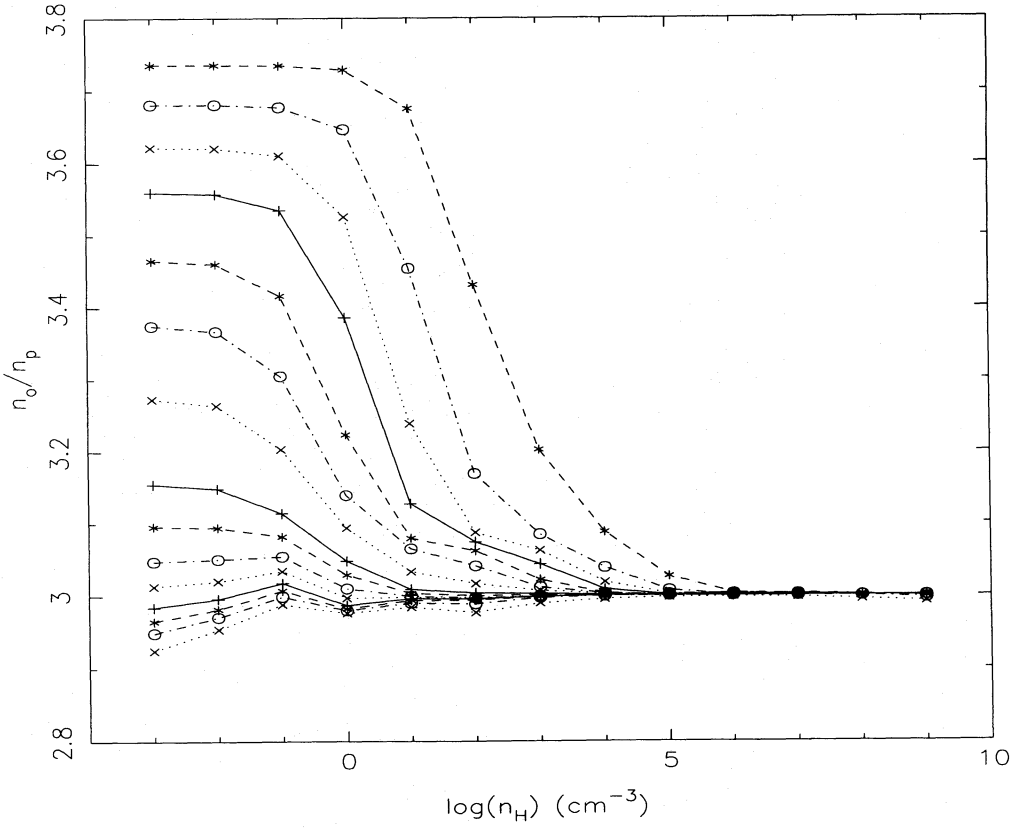

FIG. 6.—Same as Fig. 5 but for ratio of ortho to para H_2 (no analytic fit has been performed). Note that T grid begins with 450 K at the upper part of the diagram.

The left-hand equation evaluates the steady state condition $\gamma_{op} = \gamma_{po}$ in this low-density limit. The low-density ortho to para ratio is now simply $p_{(0,1)}/p_{(0,0)}$.

In the *additional* limit of very low temperature, it is often assumed that only the transitions between $k \equiv (0, 1)$ and (0, 0), respectively, are significant in equation (7). Then by detailed balance for the state-to-state $\gamma_{(0,1),(0,0)}$ and its inverse counterpart the ratio $p_{(0,1)}/p_{(0,0)}$ (whence the ortho to para ratio) would be $9 \exp(-170.5/T)$ (Mandy & Martin 1993). Note that at low temperature this low-density approximation would give precisely the same value as the thermal equilibrium ratio (the factor 9 is misprinted as 3 in eq. [2] of Flower & Watt 1984.) At 450 K this approximation would give a ratio 6.2. But the energy of state (0, 2) relative to (0, 1) is equivalent to 339.5 K and so this low-temperature limit is not reached on our grid (450 K and above). Because of the accessibility of the (0, 2) state (and others) the ratio is lower than the simple low-temperature estimate, though still typically larger than 3. With increasing temperature the low-density ortho to para ratio becomes closer to 3 (and even slightly lower) as more states (in the above sums) become accessible to exchange transitions from the ground states.

3.3. *Dissociation*

In our master equation solution, H_2 dissociates as the result of collisions to the continuum of classically unbound states (CID), or through dissociative tunneling from quasi-bound states. The *total* dissociation rate coefficient for the dissociation of H_2, γ_d, is

$$\gamma_d = \gamma_{CID} + \gamma_{dt} = \sum_{k=1,348} \gamma_{349,k}\, p_k + \sum_{k:\text{quasi-bound}} r_{349,k}\, p_k/n_H \,. \quad (8)$$

Figures 7 and 8 show γ_{CID} and γ_{dt}, respectively, as functions of n_H for various T. The timescale for dissociation is $1/(\gamma_d n_H)$.

In the low-density limit, γ_{CID} corresponds to dissociation directly from (0, 0) and (0, 1), the only populated states. Therefore, an independent way of calculating γ_{CID} without integrating the master equation (and to check it) is

$$\gamma_{CID} = \gamma_{349,(0,0)}\, p_{(0,0)} + \gamma_{349,(0,1)}\, p_{(0,1)} \,, \quad (9)$$

where $p_{(0,0)}$ and $p_{(0,1)}$ are from equation (7). Similarly, since dissociative tunneling arises from quasi-bound states excited only from the ground states

$$\gamma_{dt} = \sum_{k:\text{quasi-bound}} (1 - b_k)[\gamma_{k,(0,0)}\, p_{(0,0)} + \gamma_{k,(0,1)}\, p_{(0,1)}] \,, \quad (10)$$

where $b_k = \sum_{l:E_k > E_l} A_{lk}/(r_{349,k} + \sum_{l:E_k > E_l} A_{lk})$ is the fraction of quasi-bound molecules in state k that are stabilized by the quadrupole emission. Except for the six states mentioned in § 2.2, dissociative tunneling is much more probable than quadrupole emission (branching factor $b_k = 0$), but as a refinement to the treatment in Dove & Mandy (1986a) it is important to allow for this branching to match the master equation results precisely. Equation (10) shows directly that in this low-density limit γ_{dt} is independent of n_H (see Fig. 8); this can be reconciled with equation (8) by noting that the quasi-bound populations p_k scale as n_H in this limit. At low temperatures, since slightly less energy is required to reach a quasi-bound state (which then undergoes dissociative tunneling) than for direct CID, $\gamma_{dt} > \gamma_{CID}$. This inequality is reversed at grid temperature 4500 K and above.

With increasing density, a significant part of the dissociation takes place via "ladder climbing," a sequence of inelastic collisions in which a molecule is first excited, with interconversion of vibrational and rotational energy, and then dissociated by CID or transfer to a quasi-bound state followed by dissociative tunneling. In the master equation solution, this is represented by the increased, and now significant, steady state populations p_k of the excited states from which dissociation by either route can take place (eq. [8]).

Figure 9*a* shows the coefficients $\gamma_{349,k}$ state by state for the intermediate temperature 2000 K. Note the huge increase relative to the rate coefficient from the ground state; because of this γ_{CID} increases with density for fixed T. Internal energy is more effective in promoting dissociation than is the same amount of translational energy (Dove & Mandy 1986b), with a slight preference for the vibrational form. The latter can be seen by comparing the shapes of the contours in Figure 9*a* with those for constant internal energy in Figure 2: for a given internal energy, $\gamma_{349,k}$ is higher for higher v and lower j.

The populations p_k for $T = 2000$ K and $n_H = 10^3$ cm^{-3} have been shown in Figure 3*b*; they decrease rapidly toward the continuum, opposite to the trend for $\gamma_{349,k}$ seen in Figure 9*a*. The population-weighted contribution to γ_{CID}, $\gamma_{349,k}\, p_k$, is contoured in Figure 9*b*. For low density, all of the CID dissociation is from the ground state(s). The value 10^3 cm^{-3} is a transitional density where the highly excited *classically bound* states near the dissociation limit begin to dominate; this dominance is more pronounced with increasing density as the excited-state populations increase further. The increase of γ_{CID} with density can be seen in Figure 7, with the characteristic "critical density" behavior. The increase levels off at $n_H \sim 10^6$ cm^{-3} as the classically bound populations become collisionally dominated and stabilize.

Figure 8 shows that γ_{dt} also increases with density through a critical region and then also reaches a plateau. This plateau can be reconciled with equation (8) by recalling that the classically bound states from which the quasi-bound states are being populated have been stabilized; thus, the quasi-bound populations p_k scale as n_H just as in the low-density limit. Except in the limit of very high density where the quasi-bound states can be thermalized (well beyond our grid, which ends at $n_H = 10^9$ cm^{-3}; see § 4.2.2), dissociative tunneling *from these states* is much more probable than CID.

Also included (for the quasi-bound states) in the quantity contoured in Figure 9*b* is $r_{349,k}\, p_k/n_H$, the contribution to γ_{dt}. CID is negligible from the quasi-bound states allowing an unambiguous display of the dissociative tunneling, which is seen to be very relevant; thus, $\gamma_{dt} > \gamma_{CID}$ for $T = 2000$ K and $n_H = 10^3$ cm^{-3} as already seen for all n_H from Figures 7 and 8. Individual quasi-bound states tend to make comparable contributions to γ_{dt} despite vastly different populations, since those quasi-bound states with high tunneling probabilities have low steady state populations and conversely. It is more a matter of how quickly they are populated by collision from the lower lying bound states; as seen in Figure 9*b*, the maximum contribution is from (0, 33) and other low-lying quasi-bound states like (7, 21), which

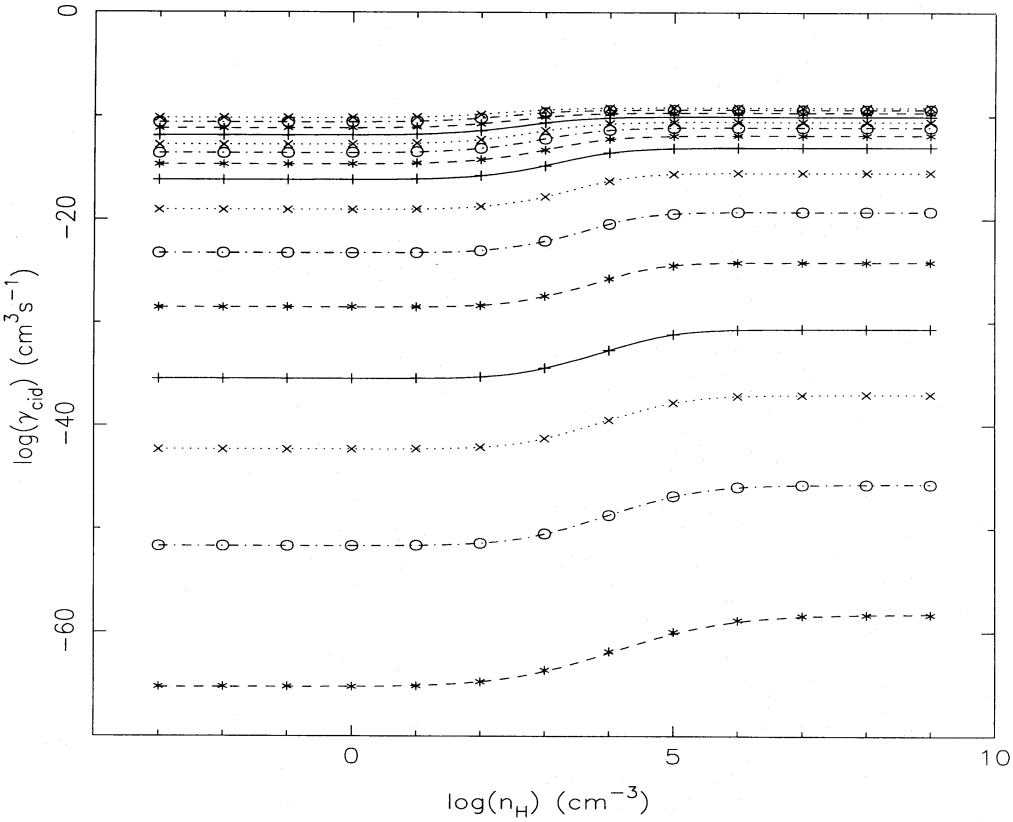

FIG. 7.—Same as Fig. 5 but for rate coefficient γ_{CID} for collision-induced dissociation

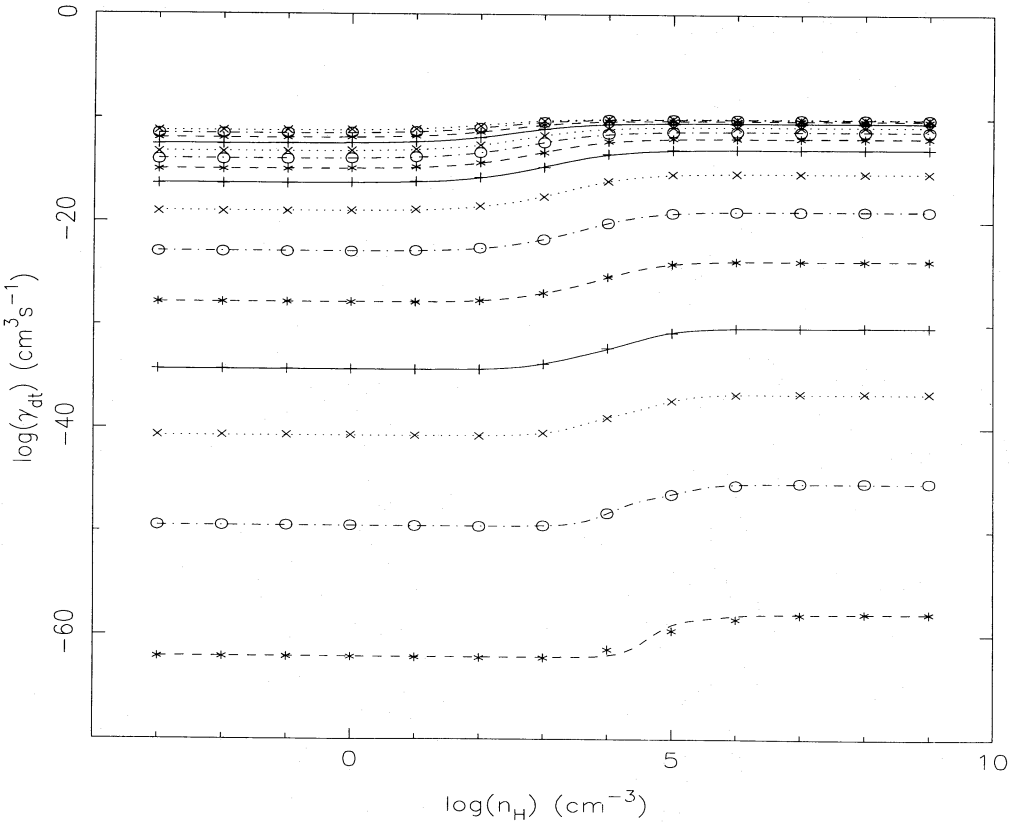

FIG. 8.—Same as Fig. 5 but for rate coefficient γ_{dt} for dissociative tunneling

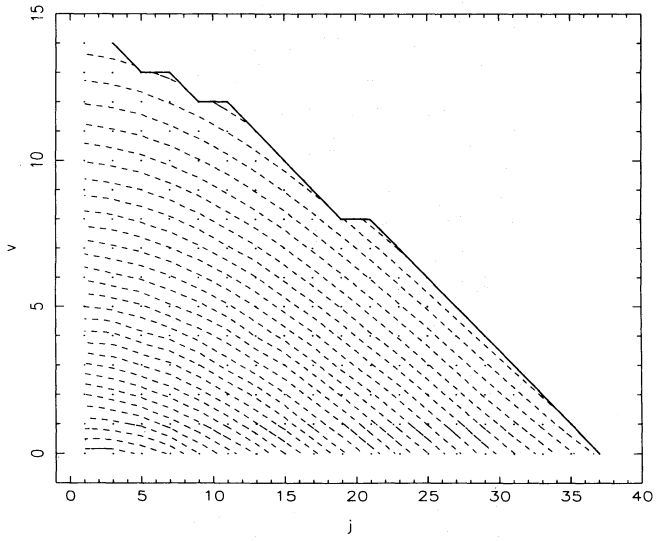

FIG. 9*a*

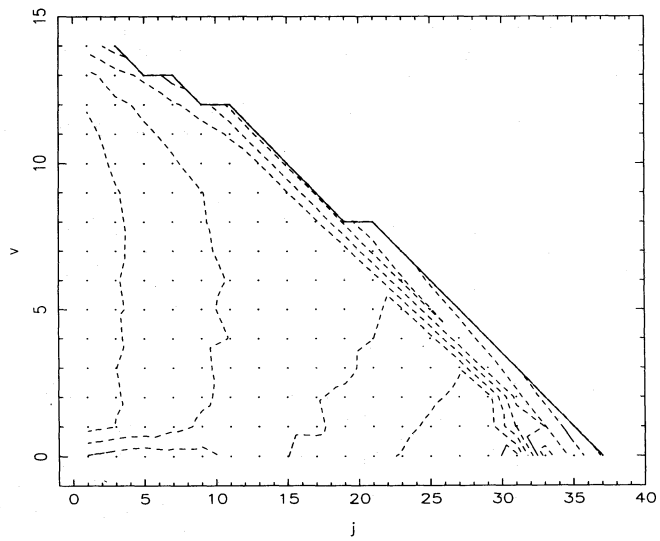

FIG. 9*b*

FIG. 9.—(*a*) Contour plot of the CID rate coefficient $\gamma_{349,k}$ (for ortho states of H_2) at $T = 2000$ K. Contours are at 0.5 dex intervals, decreasing from a value 10^{-9} cm^3 s^{-1} at the upper left to 10^{-23} cm^3 s^{-1} at the lower left. (*b*) Contour plot of the population-weighted contributions $\gamma_{349,k} p_k + r_{349,k} p_k/n_H$, for $n_H = 10^3$ cm^{-3} (see Fig. 3*b* for the fractional population p_k). Contours are at 0.5 dex intervals. The highest CID contributions are from the states (14, 3) and (13, 5); the contour level just below these states is $10^{-23.5}$ cm^3 s^{-1}. Contours at 10^{-24} cm^3 s^{-1} are adjacent to this and also above the local maximum at (0, 5). At $10^{-24.5}$ cm^3 s^{-1} contours loop down through (9, 9) and rise from (0, 15); contours at 10^{-25} cm^3 s^{-1} loop down through (9, 3) and rise from (0, 23). Although the CID contribution from the sparsely populated quasi-bound states is very low, the dissociative tunneling is important. The highest contours, 10^{-23} cm^3 s^{-1}, surround the states with highest dissociative tunneling contribution, (0, 33) and (6, 23).

are most easily populated at 2000 K. With increasing T, the maximum in $\gamma_{349,k} p_k$ moves to lower v and higher j and the relative importance of $r_{349,k} p_k/n_H$ decreases.

At high density the relative importance of γ_{dt} and γ_{CID} is like that at low density, although γ_{dt} is less dominant at low temperature and the reversal to $\gamma_{dt} < \gamma_{CID}$ is at grid temperature 6000 K. Compared to the temperature dependences at low density, those at higher density are compressed because transitions involving excited states are important.

Our model has excluded the effects of recombination (and fluorescence), which might significantly affect the populations of the upper states (§ 3.1). The contribution of the upper states to the value of γ_d can be significant as we have shown, and so our values should be used in other scenarios with caution. It can also be noted that the cases most likely to be affected are those with low upper state populations, and these coincide with low or negligible γ_d.

3.4. *Cooling Rates*

The translational kinetic temperature T is usually a distinct parameter of importance in characterizing the physical conditions, and so in this study cooling is considered to be a lowering of T or the removal of translational energy, E_{tr}. In general, the lowering of E_{tr} is balanced exactly by changes in the internal energy E_{ie} of the H_2 molecules (the *net* effect of collisional redistribution and dissociation, and of radiative deexcitation) and changes in the radiation field E_r through radiation by excited H_2 molecules. Since we are considering steady state populations, the translational cooling arises from the usual irreversible effects of radiative transitions and collisions leading to dissociation. The cooling rate per unit volume (units: ergs cm^{-3} s^{-1}) is usually called Λ, which we separate into components related to internal energy (Λ_{ie}) and radiation (Λ_r):

$$\Lambda = -dE_{tr}/dt = dE_{ie}/dt + dE_r/dt = \Lambda_{ie} + \Lambda_r . \quad (11)$$

We report the cooling rate using our steady state populations of H_2, which were obtained assuming that the translational temperature, T, is constant, consistent with the coolant, H_2, being infinitely dilute in the H gas. In actual applications one would want to investigate whether the steady state populations at that T would be reached on the cooling timescale (in this case $n_H kT/\Lambda$ since the energy of the trace amounts of H_2 is negligible).

3.4.1. *Internal Energy*

For steady fractional populations it follows from equation (3) that $\Lambda_{ie} = -D\, dn_{H_2}/dt$, where D is the absolute value of the average binding energy of the H_2 molecules for these populations. This result also makes intuitive sense. For steady state relative populations the internal energy of an average molecule is constant; only the number of molecules changes. Since we have not included recombination (and the accompanying heating) in our calculation, every dissociation of a hydrogen molecule permanently removes the required energy from translation. Thus, *in a steady state* Λ_{ie} is identical to what is sometimes referred to as dissociative cooling.

It is useful to define a rate coefficient $\gamma_{ie} \equiv \Lambda_{ie}/(n_H n_{H_2})$ (units: ergs cm^3 s^{-1}). In terms of previously defined coefficients for CID and dissociative tunneling (eq. [8]),

$$\gamma_{ie} = D\gamma_d . \quad (12)$$

In earlier work (see, e.g., Hollenbach & McKee 1979; Lepp & Shull 1983) a less precise definition has often been adopted, using instead of D the value D_0, the dissociation energy from the ground state (4.48 eV), and also ignoring

the contribution of dissociative tunneling to γ_d. In steady state conditions in which H_2 is excited, D can be appreciably less than D_0 (on our grid D is as small as 2.6 eV at high T and n_H). We have already discussed (§ 3.3) the importance of dissociative tunneling relative to CID and their behavior with T and n_H.

Figure 10 displays γ_{ie} in the familiar form of Figures 7 and 8. At 2000 K and below γ_{ie} is small in comparison to γ_r to be discussed next. Also γ_{ie} would be affected by neglect of recombination in the same way as γ_d, but only where γ_{ie} is negligible.

3.4.2. *Radiation*

Whenever a H_2 molecule in an excited (v, j) state emits a photon, the energy carried away by the photon is irreversibly lost from the gas system (which is assumed to be optically thin). As described in equation (13), the state-specific energy loss rate, shown in Figure 11, depends on the Einstein A-values (the sum of which is shown in Fig. 4*a*) and the energies of the photons emitted.

The bulk radiative cooling rate then arises from the products of these state-specific rates with the steady state populations (e.g., Fig. 3*b*). For example, using the populations for $n_H = 10^3$ cm^{-3} and $T = 2000$ K, we find that despite the bias seen in Figure 11 toward somewhat excited states most of the radiation comes from the lowest states because of the low excitation; there is a local maximum in energy loss rate at state (0, 7) for ortho states. As the excitation increases with density, the peak energy loss moves up to higher states—for example, to (1, 3) and (1, 5) for the ortho populations at 2000 K and $n_H = 10^6$ cm^{-3} and larger. Increased temperature of course also raises the excitation at constant density. Because of this population weighting, neglect of the potential importance of recombination for high-lying states (§ 3.1) should have little effect on Λ_r.

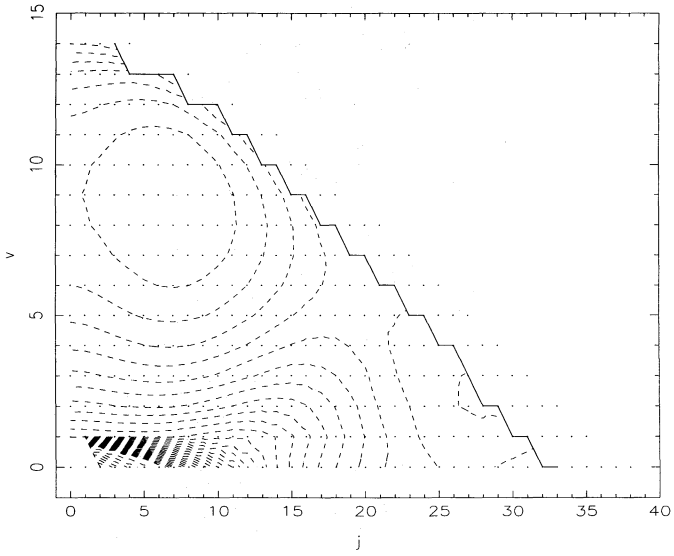

FIG. 11.—Contour plot of the radiative energy loss rate from individual (v, j) states. The first set of 29 contours are at 0.1 dex intervals, decreasing from a value 6.3×10^{-18} erg s^{-1} for the contour encircling the maximum at (9, 7); the contour passing near (4, 19) leading to a local maximum at (2, 29) is at a value 2.5×10^{-18} s^{-1}. Thereafter, in the lower left, the contour interval increases to 0.5 dex. The minimum loss rate is 2.1×10^{-24} erg s^{-1} at (0, 3).

A natural function to compute from the populations is the cooling per H_2 molecule (units: ergs s^{-1}):

$$\Lambda_r/n_{H_2} = \sum_{k=1,348} \sum_{l:E_l<E_k} (E_k - E_l) A_{lk} p_k \,. \qquad (13)$$

But for direct comparison with γ_{ie} we plot in Figure 12 the rate coefficient (units: ergs cm^3 s^{-1}) $\gamma_r \equiv \Lambda_r/(n_H n_{H_2})$.

At low densities γ_r is independent of n_H since the p_k scale linearly with n_H (§ 3.1). In this limit virtually all collisional excitations are followed by a radiative cascade to (0, 0) or (0, 1) (for the highest temperatures considered the quasi-

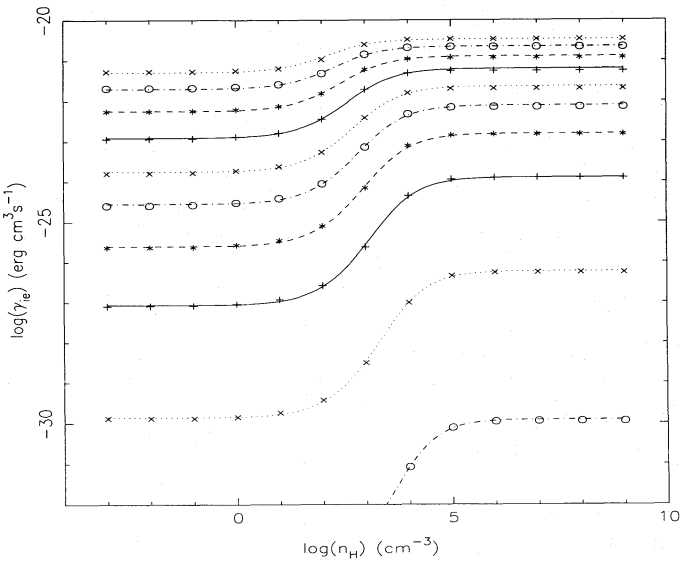

FIG. 10.—Rate coefficient γ_{ie} for the cooling contribution related to decreasing the internal energy (often called dissociative cooling for steady state conditions; see eq. [12] and also Fig. 7 for γ_{CID} and Fig. 8 for γ_{dt}). Line types and symbols are as in Fig. 5, except that results are not shown for the lowest temperatures in our grid ($T < 2000$ K). On our grid γ_{ie} is important relative to γ_r only for temperatures 3000 K and above, and even then only for n_H above the critical density (see Fig. 12).

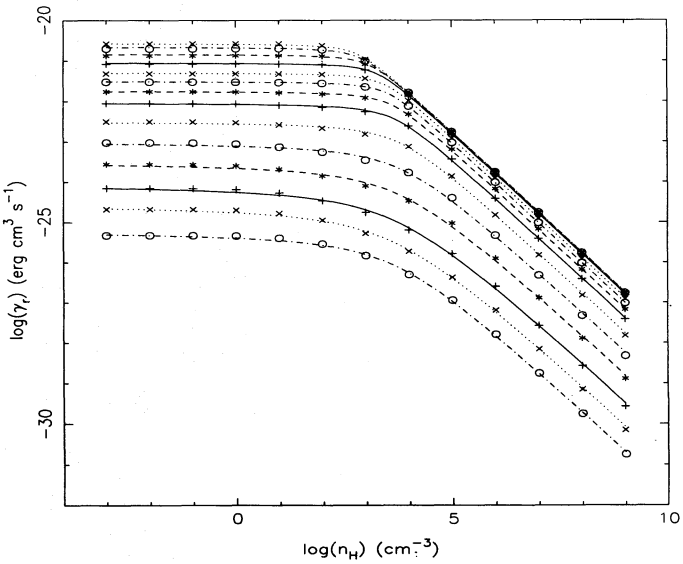

FIG. 12.—Rate coefficient γ_r for radiative cooling in same format as Fig. 10 for γ_{ie}. Lines types and symbols like Fig. 5, except that lowest locus is for 600 K. For comparison with Fig. 10, 3000 K is the second lowest dotted locus; it sinks below that for γ_{ie} at $\log(n_H) \sim 7.5$.

bound states are reached and so branching to dissociative tunneling has some effect). Therefore, in this case it is possible to calculate γ_r independently:

$$\gamma_r = \sum_{k:\text{para}} (E_k - E_{(0,0)}) b_k (\gamma_{k,(0,0)} p_{(0,0)} + \gamma_{k,(0,1)} p_{(0,1)}) \quad (14)$$

$$+ \sum_{k:\text{ortho}} (E_k - E_{(0,1)}) b_k (\gamma_{k,(0,0)} p_{(0,0)} + \gamma_{k,(0,1)} p_{(0,1)}) . \quad (15)$$

Here $p_{(0,0)}$ and $p_{(0,1)}$ are from equation (7) and b_k is the state-specific branching ratio accounting for tunneling from the quasi-bound states (see eq. [10]; $b_k = 1$ for classically bound states). Equation (14) also makes explicit that γ_r is independent of n_H in this low-density limit and that its temperature dependence arises from that of the state-to-state excitation rate coefficients.

Above the critical density collisional energy transfer becomes more influential than radiative energy transfer and steady state relative populations of the (v, j) states are reached, which no longer change with further increases in density. Therefore, at high density Λ_r/n_{H_2} does not depend on n_H and $\gamma_r \propto n_H^{-1}$. Given this decrease of γ_r with increasing n_H and the simultaneous growth of γ_{ie}, the latter comes to dominate at high densities.

4. DISCUSSION

In this section we examine the various rate coefficients derived from the master equation results in the context of previous estimates (including the low-density limit) and laboratory experiments (approximating but not identical to our high-density limit). A comparative discussion of the state-to-state collisional rate coefficients on which this study is based was presented by Mandy & Martin (1993).

4.1. *Ortho-Para Interconversion*

In many regions of interstellar space the ortho to para ratio might be modified by collisions between H_2 and protons (Dalgarno, Black, & Weisheit 1973; Flower & Watt 1984). The rate coefficient for the (0, 1) to (0, 0) transition by this process is estimated to be relatively independent of temperature and of order 3×10^{-10} cm^3 s^{-1}. This can be compared to some state-to-state values given in Mandy & Martin (1993) and the values of γ_{po} given in Figure 5 and equation (A1). For example, at 1000 K $\gamma_{po} \simeq 2 \times 10^{-13}$ cm^3 s^{-1} for a wide range of densities. Thus, at 1000 K collisions with H will come to dominate the conversion compared to collisions with H^+ when $n_{H^+}/n_H < 10^{-3}$; at 2000 K the ratio would be 10^{-2}. Thus, collisions with H are important to understanding measurements of the relative populations in the j states in warm regions (Takayanagi, Sakimoto, & Onda 1987; Tanaka et al. 1989).

Schofield (1967) has summarized some experimental measurements of the rate of conversion of para H_2 to the ortho form at high density and in the temperature range 300–450 K. Adopting Boltzmann values for the para population distribution we have used our state-to-state rate coefficients to simulate this situation; recall, however, that we regard 450 K as the lower bound on the range of validity of our coefficients. Our value is (coincidentally) within 10% of the experimental value at 450 K and a factor of 3 low at 300 K. Schofield also summarizes some theoretical calculations based on an earlier potential energy surface and extending from 300 to 1000 K. Compared to the analytic function adopted by Schofield our simulations are a factor of 2 low at 450 K, equal at 1400 K, and higher by a factor of 4 at 4500 K. Given the uncertainties, we consider the level of agreement acceptable.

4.2. *Dissociation*

4.2.1. *Comparison with Other Work*

Dalgarno & Roberge (1979) and Roberge & Dalgarno (1982) showed clearly that radiative depopulation of the higher energy states (radiative stabilization) could be significant in the interstellar medium where the density and consequently the collisional probability was sufficiently low to be comparable to the probability of quadrupole emission; their particular emphasis was on the accompanying depression of the rate of collision-induced dissociation (CID). Lepp & Shull (1983) refined the model for a warm gas ($T > 1000$ K) by including vibrationally excited states and dissociation from all vibrational levels. Not surprisingly, different sets of rate coefficients and different levels of approximation in the solution of the master equation have led to discordant estimates of the rates of CID (and cooling; § 4.3).

Figure 13 displays our results for γ_{CID} as a function of T for $n_H = 10^{-3}$ cm^{-3}, 10^3 cm^{-3}, and 10^9 cm^{-3} (low density, critical density, and high density, respectively: see Fig. 7). This form of display is that used by Roberge & Dalgarno (1982) and is useful in the context of the functional fits described in Appendix A. Also shown for comparison are values from the study by Lepp & Shull (1983) for the same densities. As pointed out earlier by Dove et al. (1987), the temperature dependence at low density is incorrect. Furthermore, the critical density that arises from their adopted excitation rate coefficients is too high, so that their results for $n_H = 10^3$ cm^{-3} are too close to those for the low-density limit. Mac Low & Shull (1986) published a modification to

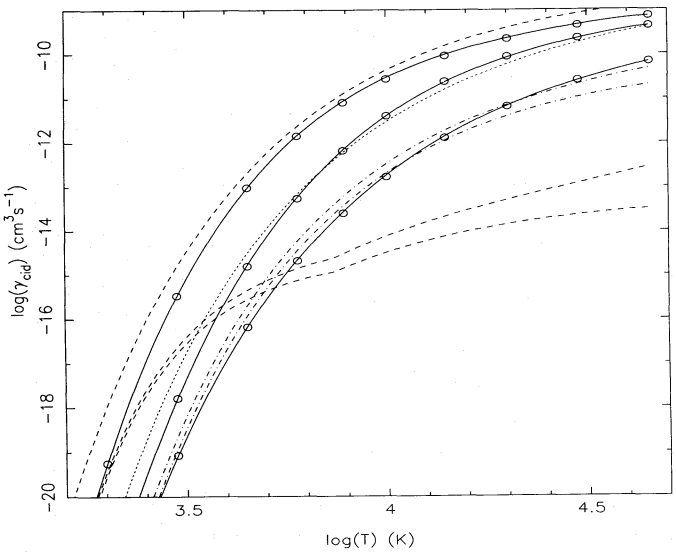

FIG. 13.—Rate coefficient γ_{CID} for collision-induced dissociation as a function of T for fixed densities. *Circles*: our values for $n_H = 10^{-3}$ cm^{-3} (*lowest curve*), 10^3 cm^{-3} (near the critical density), and 10^9 cm^{-3}. *Solid curves*: our analytic fit (eq. [A1]). *Dashed curves*: analytic form from Lepp & Shull (1983) for same densities. *Dash-dotted curves*: analytic form for two lowest densities using low-density limit from Mac Low & Shull (1986), experimental high-density limit from Breshears & Bird (1973) (same as upper dashed curve from Lepp & Shull) and interpolation formula of Lepp & Shull. *Dotted curve*: like dash-dotted case for $n_H = 10^3$ cm^{-3}, but with critical density lowered by factor 10.

the CID rate coefficient for the low-density limit, which is in closer agreement with our results (Fig. 13). However, the discrepancies at intermediate density are still present when this is combined with the critical density formulation from Lepp & Shull (as one infers should be done). If instead we lower their critical density by 1 order of magnitude, the behavior with density becomes much closer to what we find. A lower critical density is qualitatively consistent with the differences in the treatment of collisional transitions; we included all rotational and vibrational-rotational transitions, some involving smaller amounts of energy than do the vibrational-only transitions accounted for in the calculations of Lepp & Shull.

The uppermost curve in Figure 13 is the high-density limit from the experimentally determined values of Breshears & Bird (1973), these actually being constrained only in the limited range 3500–7500 K. This limit has been adopted as a firm constraint in these earlier studies; the appropriateness of this is discussed next.

4.2.2. *The High-Density Limit*

In the "high-density" limit of this study, namely $n_H = 10^9$ cm^{-3}, collisional processes dominate relative to radiative depopulation and the populations of the bound states *approach* the Boltzmann distribution (§ 3.1). In this regime, the dissociation rate coefficient γ_d is enhanced with increasing temperature because of the increase in the populations of higher energy states. However, care must be exercised in comparing γ_d for our high-density limit with experimentally measured values of the dissociation rate coefficient (Breshears & Bird). As seen in § 3.3 dissociative tunneling can be an important process relative to CID even at $n_H = 10^9$ cm^{-3}. As the density increases many orders of magnitude further to the range characteristic of laboratory experiments, γ_{dt} fades in importance relative to γ_{CID} (see eq. [8]); we have confirmed this with some simulations with n_H as large as 10^{20} cm^{-3}.

Over the limited temperature range available for comparison, 3500–7500 K, our "high-density" values of γ_{CID} are consistently lower than those of Breshears & Bird. For example, at 4500 K we find $\gamma_{CID} = 0.97 \times 10^{-13}$ cm^3 s^{-1} compared to 2.0×10^{-13} cm^3 s^{-1}. (Values of γ_d, which include dissociative tunneling, are coincidentally very close: 2.0×10^{-13} cm^3 s^{-1} at 4500 K, for example; see also Fig. 13). Nevertheless, the agreement between experiment and our purely theoretical calculations based on ab initio CID rate coefficients $\gamma_{349,k}$ is quite remarkable, and the slight systematic discrepancies can be understood at least qualitatively. At $n_H = 10^9$ cm^{-3}, our values of γ_{CID} are low because of an underpopulation of the upper states, which have the largest individual CID rate coefficients (e.g., Fig. 9*a*). In higher density simulations, this is gradually redressed but the values for the CID rate coefficient are still slightly low. If, on the other hand, we simply take Boltzmann populations in combination with our individual CID rate coefficients $\gamma_{349,k}$ we tend to overestimate the laboratory results slightly since we have now overcompensated for the population of the upper states.

Another reason that even our highest density simulations (including some with radiative and dissociative tunneling rates set to zero) have slightly depressed populations for the important high-energy (including quasi-bound) states is that in the simulations these states are not repopulated by recombination, a process that is important at experimental densities. Schwenke (1990) has included recombination in some higher density master equation calculations based on some similar state-to-state rate coefficients. One of his models (his Fig. 3) has $n_H \simeq 2 \times 10^{16}$ cm^{-3} and $n_{H_2} < n_H$ consistent with our assumptions. For this model at 5000 K his time-dependent results show a "plateau region" at which a quasi–steady state has been established (the timescale agrees with our time-dependent integrations), before recombination has become important to the state populations. Interpolating from simulations at 4500 and 6000 K and $n_H = 10^{16}$ cm^{-3} we have been able to reproduce the dissociation rate coefficient deduced from his results for the plateau region. Thereafter, his dissociation rate coefficient increases with time by a factor 3 to a value close to the value we derive using simply Boltzmann populations.

From these considerations it can be seen that it is not appropriate to force the "high-density" limit of γ_{CID} (at $n_H = 10^9$ cm^{-3}) to match the measurements of Breshears & Bird, as has been done by Roberge & Dalgarno (1982) and Lepp & Shull (1983). Furthermore, as discussed in § 3.3, over the whole range one also has to include dissociative tunneling, which has been omitted in previous studies.

4.3. *Cooling*

Early assessments of the cooling rate focussed on the role of rotational excitation (Takayanagi & Nishimura 1960; Nishimura 1968; Elitzur & Watson 1978). For warmer gas this has to be extended by inclusion of vibrational transitions. Figure 14 displays our results for the radiative cooling rate per H_2 molecule, Λ_r/n_{H_2}, as a function of T for fixed densities and compares them to the analytic fits found by Lepp & Shull (1983; see also their Fig. 3) and Hollenbach & McKee (1979; see also their Fig. 7, which shows γ_r). The uppermost curves in Figure 14 are for the "high-density" limit for which the populations approach their Boltzmann values. Our results offer some improvement at high T owing to our complete treatment of the (v, j) states. The plateau beginning at $T = 10^4$ K does not appear for

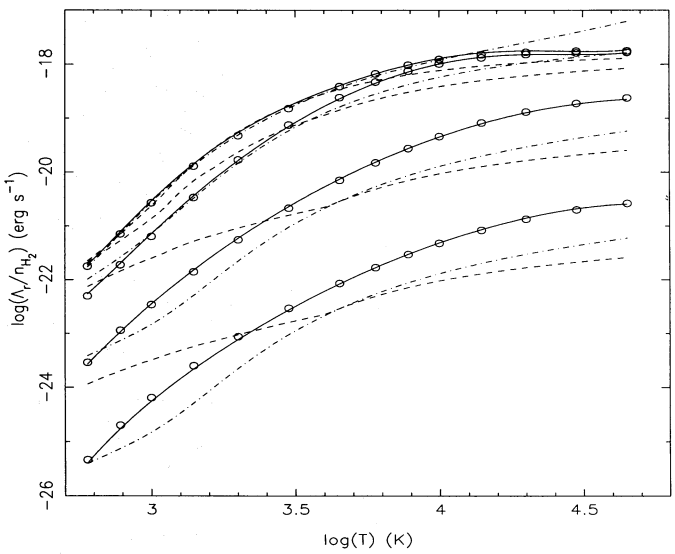

FIG. 14.—Radiative cooling rate per H_2 molecule, Λ_r/n_{H_2} as a function of T for fixed densities: $n_H = 10^0$ cm^{-3} (*lowest curve*), 10^2 cm^{-3}, 10^4 cm^{-3} and 10^8 cm^{-3} ("high-density" limit). *Solid curves*: our analytic fit (eq. [A2]). *Dashed curves*: analytic form from Lepp & Shull (1983). *Dash-dotted curves*: analytic form from Hollenbach & McKee (1979).

Boltzmann populations, but occurs in our master equation results because the high-energy states near the dissociation limit remain somewhat underpopulated as discussed in § 3.1. Larger differences with respect to the earlier results occur for lower densities. At the lowest densities, where γ_r becomes independent of n_H (Fig. 12; eq. [14]), the differences can be attributed to use of different excitation rate coefficients from the ground states and detailed inclusion of a full suite of excited states. Our results show that at intermediate densities, a full master equation solution is required to determine the populations of all states.

4.4. *Conclusions*

Over the past two decades computational speeds have improved to the extent that it should be possible to include a full treatment of the (v, j) populations of H_2 in models of astrophysically interesting environments, like shocks and photodissociation regions. Our models illustrate this possibility for time-dependent calculations (which in our case lead to steady state conditions) and show that a full simulation is a desirable goal compared to approximate treatments. Over the same time there have been significant advances in the computation of the potential energy surface for $H + H_2$ and in the calculation of state-to-state (and CID) cross sections, to the point that a full set of state-to-state rate coefficients is now available for the $H + H_2$ interaction (Mandy & Martin 1995; Martin & Mandy 1995) at intermediate temperatures. These rate coefficients need to be extended by quantum calculations to lower temperatures, which is not insurmountable since there only the lowest (v, j) states are important. Among the remaining challenges is development of a set of state-to-state rate coefficients for the $H_2 + H_2$ interaction.

This work was supported by the Natural Sciences and Engineering Research Council of Canada. We thank R. J. LeRoy for an electronic version of the dissociative tunneling probabilities and the referee for insightful comments.

APPENDIX

FUNCTIONAL APPROXIMATIONS

The following fits have been made and are available in electronic form (see Appendix C).

APPENDIX A

COLLISIONAL RATE COEFFICIENTS

Figure 5 (γ_{po}), Figure 7 (γ_{CID}), Figure 8 (γ_{dt}), and Figure 10 (γ_{ie}) show that the respective rate coefficients all have qualitatively similar behavior. For fixed temperature there is a flat portion at low density, say γ_l, and another higher flat portion at high density, say γ_h. The transition occurs near some critical density n_c. This motivates the following form, generalized from Lepp & Shull (1983):

$$\log \gamma_{h,1} = \alpha_1 + \alpha_2 \log T + \alpha_3(\log T)^2 + \alpha_4(\log T)^3 + \alpha_5 \log (1 + \alpha_6/T) , \qquad \log \gamma_{h,2} = \alpha_7/T ,$$

$$\log \gamma_{l,1} = \alpha_8 + \alpha_9 \log T + \alpha_{10}(\log T)^2 + \alpha_{11} \log (1 + \alpha_{12}/T) , \qquad \log \gamma_{l,2} = \alpha_{13}/T ,$$

$$\log n_{c,1} = \alpha_{14} + \alpha_{15} \log T + \alpha_{16}(\log T)^2 + \alpha_{17}/T , \quad p = \alpha_{19} + \alpha_{20} \exp (-T/1850) + \alpha_{21} \exp (-T/440) ,$$

$$\log n_{c,2} = \alpha_{18} + \log n_{c,1} ,$$

$$\log \gamma = \log \gamma_{h,1} - (\log \gamma_{h,1} - \log \gamma_{l,1})/[1 + (n_H/n_{c,1})^p] + \log \gamma_{h,2} - (\log \gamma_{h,2} - \log \gamma_{l,2})/[1 + (n_H/n_{c,2})^p] . \quad \text{(A1)}$$

At density n_c, γ is the geometric mean of γ_l and γ_h.

Table 1 contains the α's. Units for these parameters are not given but are obvious from the context (c.g.s. units; see axis labels in figures and footnotes to the table). These parameters were obtained by nonlinear least-squares fits to the computed grid of values for each rate coefficient (low- and high-density limits were not optimized separately). Grid values at 450 K were given low weight except in the case of γ_{po}, and so the fits should be used with caution below 600 K. To indicate the quality of the fit, the *rms* error along with the maximum and minimum (signed) deviation (within the valid T range) are also tabulated (all in percent).

APPENDIX B

RADIATIVE COOLING RATE

Figure 11 for $\log \gamma_r$ shows a qualitatively different behavior with respect to n_H and T. At low density there is a flat portion that turns downward at some critical density n_c to a high-density linear portion with slope -1. This motivates use of a

TABLE 1

ANALYTIC FITS OF STEADY STATE RATE COEFFICIENTS FOR $H + H_2$

Fit	γ_{po}[a]	γ_{CID}[a]	γ_{dt}[a]	γ_{ie}[b]	γ_r[b]
rms[c]	1.6	3.9	8.7	6.9	7.5
max[c]	3.6	9.3	23.8	31.3	19.1
min[c]	−4.0	−8.8	−20.4	−17.5	−19.8
1[d]	1.045999+2	−1.784239+2	−1.427664+2	−1.846781+2	−1.058656+3
2	−5.180703+1	−6.842243+1	4.270741+1	3.793892+1	6.412920+2
3	7.374957+0	4.320243+1	−2.027365+0	2.996993+0	−1.330667+2
4	−3.123496−1	−4.633167+0	−2.582097−1	−8.286897−1	9.285717+0
5	−1.621112+1	6.970086+1	2.136094+1	3.155289+1	9.160106+1
6	1.029437+4	4.087038+4	2.753531+4	2.861577+4	2.680075+3
7	−2.606107+3	−2.370570+4	−2.146779+4	−2.141734+4	9.500433+3
8	−1.733190+0	1.288953+2	6.034928+1	6.265847+1	−1.253746+3
9	−2.417648+0	−5.391334+1	−2.743096+1	−3.282533+1	7.792906+2
10	1.532729−1	5.315517+0	2.676150+0	3.275816+0	−1.628687+2
11	−2.409915+0	−1.973427+1	−1.128215+1	−1.351127+1	1.145088+1
12	2.284705+4	1.678095+4	1.425455+4	1.430836+4	1.057438+2
13	−1.626040+3	−2.578611+4	−2.312520+4	−2.309884+4	2.889762+3
14	3.061327+1	1.482123+1	9.305564+0	5.903307+0	1.382858+4
15	−1.154976+1	−4.890915+0	−2.464009+0	−7.783954−1	−1.175497+2
16	1.177836+0	4.749030−1	1.985955−1	−6.723144−3	7.886144+1
17	−3.924553+3	−1.338283+2	7.430600+2	8.954974+2	−1.777082+1
18	−1.684643−1	−1.164408+0	−1.174242+0	−1.156336+0	1.338843+0
19	7.329367−1	8.227443−1	7.502286−1	8.040080−1	3.406424+3
20	−7.165353−1	5.864073−1	2.358848−1	1.464416−1	...
21	−4.441274−1	−2.056313+0	2.937507+0	2.615630+0	...

[a] Units: $cm^3\ s^{-1}$.
[b] Units: ergs $cm^3\ s^{-1}$.
[c] The rms, maximum, and minimum of signed deviations in percent.
[d] Coefficients α_i for analytic fits.

hyperbola to describe the data at fixed T, whence

$$\log \gamma_h = -\log n_H + \alpha_1 + \alpha_2 \log T + \alpha_3(\log T)^2 + \alpha_4(\log T)^3 + \alpha_5 \log (1 + \alpha_6/T) + \alpha_7/T ,$$

$$\log \gamma_l = \log \gamma_h + \log n_H - \log n_c , \qquad f = \log \gamma_l/\gamma_h \equiv \log n_H/n_c ,$$

$$\log n_c = \alpha_8 + \alpha_9 \log T + \alpha_{10}(\log T)^2 + \alpha_{11}(\log T)^3 + \alpha_{12} \log (1 + \alpha_{13}/T) + \alpha_{14}/T ,$$

$$w = \alpha_{15} + \alpha_{16} \log T + \alpha_{17}(\log T)^2 + \alpha_{18}(\log T)^3 + \alpha_{19}/T ,$$

$$\log \gamma_r = \log \gamma_h + 0.5[f - (f^2 + 2w^2)^{1/2}] . \qquad \text{(A2)}$$

The fit is summarized in Table 1, again for 600 K and above. The low- and high-density limits, γ_l and γ_h, were not optimized separately.

APPENDIX C

AVAILABILITY IN ELECTRONIC FORM

The following is a description of several files and associated test programs that may be requested by e-mail.

A file from which the entries in Table 1 were made is available, along with a test program (in FORTRAN) that reads this file and evaluates the various coefficients as a function of temperature and density using equations (A1) and (A2).

The data assembled for solution of the master equation (eqs. [1] and [2]) were described in § 2. The population n_l on the right-hand side of the master equation is an element of a column vector of length 348 + 1. The elements were ordered as follows. First come the 177 para-H_2 (v, j) states, with an inner loop on v (vertically in Fig. 1):

(0, 0), (1, 0), (2, 0), ..., (14, 0), (0, 2), (1, 2), ..., (0, 34), (1, 34), (0, 36), (0, 38).

Then come the 171 ortho-H_2 (v, j) states:

(0, 1), (1, 1), (2, 1), ..., (14, 1), (0, 3), (1, 3), ..., (0, 35), (1, 35), (0, 37).

Element 349 corresponds to a dissociated molecule. Subroutines to translate from (v, j) to l and vice versa are available. These can be exercised with a test program that reads a file of the energies of the (v, j) states (as plotted in Fig. 1) to generate (elements of) the corresponding energy column vector.

With the above ordering the matrix of elements A_{kl} (radiative transition probabilities from state l) contains two square blocks on the diagonal of dimensions 177 and 171 since there are no parity-changing quadrupole radiative transitions. Each block is sparse because of selection rules on Δj. Row and column 349 are empty. A test program to produce this matrix is available.

The dissociative tunneling transition probabilities $r_{349,l}$ can be regarded as row 349 of an otherwise empty matrix. Even this row is zero except for the quasi-bound states. In the test program it is added to the matrix A_{kl}, which had row 349 empty.

In the test program a diagonal element A_{kk} corresponding to the sum of all radiative and dissociative tunneling transitions out of each of the 348 states k is generated as the negative of the sum along that column.

Electronic files of the matrix γ_{kl} with this same ordering have been made available separately (Martin & Mandy 1995).

REFERENCES

Black, J. H., & Dalgarno, A. 1976, ApJ, 203, 132
Black, J. H., Porter, A., & Dalgarno, A. 1981, ApJ, 249, 138
Blais, N. C., & Truhlar, D. G. 1979, J. Chem. Phys., 70, 2962
Blais, N. C., Truhlar, D. G., & Mead, C. A. 1988, J. Chem. Phys., 89, 6204
Boothroyd, A. I., Keogh, W. J., Martin, P. G., & Peterson, M. R. 1991, J. Chem. Phys., 95, 4343,
———. 1996, J. Chem. Phys., submitted
Breshears, W. D., & Bird, P. F. 1973, in 14th Symp. (Int.) on Combustion (Pittsburgh: Combustion Institute), 211
Burton, M. G., Hollenbach, D., & Tielens, A. G. G. M. 1990, ApJ, 365, 620
Chang, C. A., & Martin, P. G. 1991, ApJ, 378, 202
Dalgarno, A., Black, J. H., & Weisheit, J. C. 1973, Astrophysical Lett., 14, 77
Dalgarno, A., & Roberge, W. G. 1979, ApJ, 233, L25
Dove, J. E., & Mandy, M. E. 1986a, ApJ, 311, L93
———. 1986b, Int. J. Chem. Kinetics, 18, 993
Dove, J. E., Rusk, A. C. M., Cribb, P. H., & Martin, P. G. 1987, ApJ, 318, 379
Duley, W. W., & Williams, D. A. 1986, MNRAS, 223, 177
Elitzur, M., & Watson, W. D. 1978, A&A, 70, 443
Flower, D., & Watt, G. D. 1984, MNRAS, 209, 25
Fox, L., & Wilkinson, J. H. 1990, The NAG Fortran Library Manual, Mark 14 (Oxford: NAG Ltd.)
Hollenbach, D., & McKee, C. F. 1979, ApJS, 41, 555
———. 1989, ApJ, 342, 306
Keogh, W. J., Boothroyd, A. I., Martin, P. G., Mielke, S. L., Truhlar, D. G., & Schwenke, D. W. 1992, Chem. Phys. Lett., 195, 144
Lepp, S., Buch, V., & Dalgarno, A. 1995, ApJS, 98, 345
Lepp, S., & Shull, J. M. 1983, ApJ, 270, 578
LeRoy, R. J., & Bernstein, R. B. 1971, J. Chem. Phys., 54, 5114
Liu, B. 1973, J. Chem. Phys., 58, 1925
Mac Low, M., & Shull, J. M. 1986, ApJ, 302, 585
Mandy, M. E., & Martin, P. G. 1991, J. Phys. Chem., 95, 8726
———. 1992, J. Chem. Phys., 97, 265
———. 1993, ApJS, 86, 199
———. 1996, in preparation
Martin, P. G., & Mandy, M. E. 1995, ApJ, 455, L89
Nishimura, S. 1968, Ann. Tokyo Astron. Obs. Ser. 2, 11, 33
Roberge, W., & Dalgarno, A. 1982, ApJ, 255, 176
Schofield, K. 1967, Planet. Space Sci., 15, 643
Schwartz, C., & LeRoy, R. J. 1987, J. Mol. Spectrosc., 121, 420
Schwenke, D. W. 1990, J. Chem. Phys., 92, 7267
Siegbahn, P., & Liu, B. 1978, J. Chem. Phys., 68, 2457
Shapiro, P. 1992, in Astrochemistry of Cosmic Phenomena, ed. P. D. Singh (Dordrecht: Kluwer), 73
Sternberg, A., & Dalgarno, A. 1989, ApJ, 338, 197
———. 1995, ApJS, 99, 565
Sun, Y., & Dalgarno, A. 1994, ApJ, 427, 1053
Takayanagi, K., & Nishimura, S. 1960, PASJ, 12, 77
Takayanagi, K., Sakimoto, K., & Onda, K. 1987, ApJ, 318, L81
Tanaka, M., Hasegawa, T., Hayashi, S. S., Brand, P. W. J. L., & Gatley, I. 1989, ApJ, 336, 207
Tielens, A. G. G. M., & Hollenbach, D. M. 1985, ApJ, 291, 722
Truhlar, D. G., & Horowitz, C. J., 1978, J. Chem. Phys., 68, 2466; erratum 71, 1514E (1979)
Turner, J., Kirby-Docken, K., & Dalgarno, A. 1977, ApJS, 35, 281
Varandas, A. J. C., Brown, F. B., Mead, C. A., Truhlar, D. G., & Blais, N. C., 1987, J. Chem. Phys., 86, 6258
Wagenblast, R., & Hartquist, T. W. 1989, MNRAS, 237, 1019
Wu, Y. M., & Kuppermann, A. 1993, Chem. Phys. Letters, 201, 178